



OPEN ACCESS

EDITED BY

Kanikkai Raja Aseer,
National Institute on Aging (NIH),
United States

REVIEWED BY

Allwin Jennifa Silvester,
National Institute on Aging (NIH),
United States
Sumei Liu,
University of Wisconsin–La Crosse,
United States

*CORRESPONDENCE

Eunok Im

✉ eoim@pusan.ac.kr

RECEIVED 16 June 2023

ACCEPTED 11 August 2023

PUBLISHED 25 August 2023

CITATION

Lee Y, Kim Y, Park S, Heo G, Chung HY and Im E (2023) Cannabinoid receptor type 1 in the aging gut regulates the mucosal permeability via miR-191-5p. *Front. Endocrinol.* 14:1241097. doi: 10.3389/fendo.2023.1241097

COPYRIGHT

© 2023 Lee, Kim, Park, Heo, Chung and Im. This is an open-access article distributed under the terms of the [Creative Commons Attribution License \(CC BY\)](#). The use, distribution or reproduction in other forums is permitted, provided the original author(s) and the copyright owner(s) are credited and that the original publication in this journal is cited, in accordance with accepted academic practice. No use, distribution or reproduction is permitted which does not comply with these terms.

Cannabinoid receptor type 1 in the aging gut regulates the mucosal permeability via miR-191-5p

Yunna Lee^{1,2}, Yuju Kim¹, Soyeong Park^{1,2}, Gwangbeom Heo^{1,2}, Hae Young Chung^{1,2} and Eunok Im^{1,2*}

¹College of Pharmacy, Pusan National University, Busan, Republic of Korea, ²Research Institute for Drug Development, Pusan National University, Busan, Republic of Korea

Background: Aging is associated with a broad loss of function throughout the body, and gastrointestinal (GI) dysfunction can occur with aging. The endocannabinoid (eCB) system plays a pivotal role in various GI diseases, and alterations in the eCB system have been observed during brain and skin aging. Therefore, we investigated the putative role of the eCB system in aging-related changes in the intestine.

Methods: The expression of cannabinoid receptor type 1 (CB₁) was investigated in rat intestinal tissues using quantitative real-time PCR. Cellular senescence was induced by hydrogen peroxide (H₂O₂) and hydroxyurea (HU) in rat and human intestinal epithelial cells. Cellular permeability was evaluated by transepithelial electrical resistance (TEER) measurement.

Results and Discussion: The expression of CB₁ was decreased in the small intestine of aged rats compared to that of young rats. Senescent cells showed reduced TEER values and decreased expression of ZO-1, indicating increased intestinal permeability, which is tightly regulated by the CB₁ signaling. *In silico* miRNA analysis suggested that ZO-1 was a direct target gene of miR-191-5p. Increased expression of miR-191-5p by HU was restored by CB₁ agonist ACEA co-treatment. Moreover, NF-κB p65 activation was associated with CB₁-related miR-191-5p signaling. In conclusion, aging-induced CB₁ reduction leads to increased intestinal permeability and decreased ZO-1 expression via upregulation of miR-191-5p and NF-κB p65 activation. Taken together, these results suggest that CB₁ signaling may be a useful strategy to reduce intestinal permeability in aging-related and other inflammatory conditions in the gut.

KEYWORDS

aging gut, endocannabinoid, CB₁, miR-191-5p, intestinal permeability

Introduction

The increase in the aged population is a global demographic trend. Aging is associated with a physiological decline and widespread loss of function in the body. The gastrointestinal (GI) tract is one of the most complex organ systems, which performs diverse functions that are essential to life. GI disorders due to aging are directly related to the quality of life and morbidity in the older population because multiple functions of the GI tract, such as secretion, digestion, absorption, excretion, and defense, are critical for maintaining general health in the body (1).

One of the important factors that cause age-related intestinal diseases is impaired function of the intestinal mucosal barrier in the elderly population (2). An intact intestinal barrier allows the peaceful coexistence of the intestinal microbiota without an immune response; it induces an effective exchange of molecules between the host and the environment and mediates efficient absorption of nutrients (3). Moreover, the intestinal barrier is the first line of defense against external environments and pathogens, mainly from the food ingestion. In this reason, age-associated modifications of intestinal epithelial barrier leads to the detrimental effects such as a decline of innate immune response to pathogenic stimulus (4). Generally, normal intestinal permeability in healthy individuals can be defined by the proper distribution and location of tight junction proteins, such as zonula occludens-1 (ZO-1), claudins, and occludins (5). However, age-associated changes in tight junction proteins loosen the intestinal barrier, increase intestinal permeability, and elevate the level of pro-inflammatory cytokines (6).

Recent studies have shown that the endocannabinoid (eCB) system plays a key role in regulating intestinal permeability. The eCB system is composed of not only endogenous cannabinoids, such as ligands and two G protein-coupled receptors (GPCRs), including cannabinoid receptor type 1 (CB₁) and cannabinoid receptor type 2 (CB₂), but also includes bioactive enzymes associated with the biosynthesis and degradation of eCBs (7). In a study using intestinal epithelial-derived Caco-2 cancer cell lines, the eCB system modulated intestinal permeability by altering the expression levels of ZO-1 and claudin-1 (8). This suggests that eCB system may play a role in modulating intestinal permeability by regulating the expression of tight junction proteins.

Emerging evidence suggests that the eCB system undergoes age-dependent changes. In rodents, mRNA levels of CB₁ and CB₂ agonists in the brain are relatively high in adults but markedly reduced in older animals (9). A study on the human brain also indicated that the expression level of the CB₁ is significantly higher in younger than that in older individuals (10). Age-related reduction in the eCB system has been linked to decreased food intake in aged animals and age-related decline in learning and memory abilities in CB₁-deficient mouse models (11, 12). As the CB₁ is also expressed in peripheral organs, it is thought that the eCB system regulates the aging process in extraneural tissues. For example, CB₁-knockout mice undergo changes that resemble skin aging in their skin structure (13). Therefore, alterations in CB₁ expression are closely associated with aging in both the brain and peripheral tissues. However, the role of the eCB system in the aging gut has not been studied.

Accordingly, the primary objectives of this study were to (1) investigate the physiological functions of CB₁ signaling in age-related intestinal alterations, especially focusing on intestinal permeability and (2) to uncover the underlying mechanism by which microRNAs (miRNAs) are involved in CB₁ signaling in the aged intestine.

Materials and methods

Animals

Pathogen-free male Sprague Dawley rats were obtained from Samtako (Osan, South Korea) and fed a standard laboratory diet (Superfeed Co., Wonju, Gangwon, South Korea) *ad libitum*. Animals aged 6 and 24 months were used as young and old rats (n=10), respectively. All animal studies were designed by the Aging Tissue Bank and approved by the Institutional Animal Care Committee of the Pusan National University. We thank the Aging Tissue Bank for providing aging tissues. We followed the guidelines for animal experiments issued by the Pusan National University (Approval Number PNU-2012-0088).

Cell culture & *in vitro* cell senescence model

Normal rat small intestinal epithelial cells (IEC-6; cat. no. CRL-1592) and the human colonic epithelial adenocarcinoma cell line Caco-2 (cat. no. HTB-37TM) were purchased from American Type Culture Collection (Manassas, VA, USA). Cells were cultured in Dulbecco's modified Eagle's medium (DMEM) with high glucose (4.5 g/L), 10% heat-inactivated fetal bovine serum, and 100 units/ml penicillin, and 100 µg/ml streptomycin solution (all from Hyclone Laboratories, Logan, UT, USA) at 37 °C in a 5% CO₂ air environment. The medium was changed every alternate day.

To induce *in vitro* cell senescence, IEC-6 cells were treated with hydrogen peroxide (H₂O₂) (Duksan Pure Chemicals, Gyeonggi-do, South Korea) for 2 h to induce oxidative stress. H₂O₂ was diluted in DMEM to 50, 100, and 150 µM. After treatment with H₂O₂ for 2 h, the cultures were rinsed twice with phosphate-buffered saline (PBS) and incubated in DMEM for 24–72 h. To establish another *in vitro* cell senescence model, Caco-2 cells were treated with 150 µM hydroxyurea (HU, cat. no.; H-8627; Sigma-Aldrich, St Louis, MO, USA) for 48 h without changing the culture medium. To inhibit CB₁ signaling, IEC-6 cells and Caco-2 cells were treated with 2 µM of CB₁ inverse agonist SR141716A (Tocris Bioscience, Bristol, UK) after H₂O₂ exposure in IEC-6 cells and during HU treatment in Caco-2 cells. In contrast, pretreatment with the CB₁ agonist arachidonyl-2'-chloroethylamide (ACEA) was used to reinforce the agonist activity. Cells were pretreated with 10 µM ACEA (Tocris Bioscience) for 30 min before H₂O₂ or HU-induced cell senescence and incubated for 48 h. To measure morphological changes in IEC-6 cells and Caco-2 cells after treatment with H₂O₂ and HU, cells were observed under a microscope and photographed using a Nikon ECLIPSE TE 2000-U microscope (Nikon, Tokyo, Japan).

Senescence-associated β -galactosidase activity

SA- β -gal positive cells were assessed using a senescence detection kit (Cell Signaling Technologies, Danvers, MA, USA), according to the manufacturer's instructions. Briefly, 1×10^5 cells were seeded in six-well culture plates and stabilized for 48 h. After stabilization, cells were exposed to oxidative stress induced by H_2O_2 and HU. After treatment with H_2O_2 for 2 h, the cultures were rinsed twice with PBS and incubated in DMEM for 24–72 h. HU treatment was maintained for 6 d to obtain a clearer senescence-like phenotype. After treatment, the cells were washed with PBS and fixed for 15 min in a fixative solution. The fixed cells were then washed twice with PBS and incubated with β -galactosidase staining solution at 37 °C overnight. After staining, images from five random microscopic fields were acquired using a camera-equipped bright-field microscope (Nikon ECLIPSE TE 2000-U microscope). SA- β -gal-positive cells can be easily determined by counting the number of blue cells in the total population.

Quantitative polymerase chain reaction & reverse transcription PCR

Total RNA was isolated from rat tissues and cells using the TRIzol RNA extraction method (Ambion, Thermo Scientific, Waltham, MA, USA). RNA samples (1,000 ng) were reverse-transcribed to complementary DNA (cDNA) using the RT & GO master mix (MPbio, Santa Ana, CA, USA) and oligo (dT) primers (ELPIS-Biotech, Daejeon, South Korea). To detect CB_1 and CB_2 expression in both rat tissues, rat cells and human cells, qPCR was performed using a Thermal Cycler TP800 (TAKARA, Kusatsu, Japan). Primers used for the qPCR were designed manually and the sequences were shown in Table 1. After amplification, the results were analyzed using a Thermal cycler dice real time system v5 (TAKARA). The $\Delta\Delta C_t$ method was used to analyze mRNA expression. RT-PCR was conducted to confirm the expression of tight junction proteins in senescent cells using manually designed primer sequences (Table 1). The first cDNA strand was amplified using the Maxime PCR PreMix (iNtRON Biotechnology, Gyeonggi-do, South Korea) with initial denaturation for hot-start (94 °C, 10 min), 35 cycles of denaturation (94 °C, 1 min), primer annealing (53 °C, 1 min), extension (72 °C, 45 s), and final extension (72 °C, 10 min).

Hematoxylin and eosin staining

Segments of the excised colon and small intestine were fixed in 10% buffered formalin solution (Sigma-Aldrich), embedded in paraffin, and stained with H&E. Histological changes were observed using a microscope (Olympus Corp., Tokyo, Japan), photographed with a Moticam 3.0MP Color Digital Camera (Motic, Causeway Bay, Hong Kong), and analyzed using motic images plus 2.0 software.

TABLE 1 PCR primer sequences.

Genes	Sequences (5'-3')
rat CB_1	F: GCT GAA CTC CAC CGT GAA CC
	R: CGA AGC ATG TTC CCT TCG TG
rat CB_2	F: CCT TCA CGG CCT CTG TGG
	R: CGG CGT TGA TCT CCT ACC TAC
rat ZO-1	F: AGC GAA GCC ACC TGA AGA TA
	R: GAT GGC CAG CAG GAA TAT GT
rat ZO-2	F: TAA AGG TGA AAC CGT GAC CA
	R: CAC AGG CCA GGA TGT CTC TA
rat claudin-2	F: TCT GGA TGG AGT GTG CGA C
	R: AGT GGC AAG AGG CTG GGC
rat claudin-4	F: CTC TCG CCT CCA CGT TAC TC
	R: AGG GTA GGT GGG TGG GTA AG
rat occludin	F: CTG TCT ATG CTC GTC ATC G
	R: CAT TCC CGA TCT AAT GAC GC
rat GAPDH	F: TGC TGG TGC TGA GTA TGT CG
	R: AGT TGG TGG TGC AGG ATG C
human CB_1	F: TGG AAC TGC GAG AAA CTG CA
	R: ACA GAA GCA GTA CGC TGG TG
human GAPDH	F: CGC TCT CTG CTC CTC CTG TT
	R: CCA TGG TGT CTG AGC GAT GT

Immunohistochemistry and immunofluorescence staining

For IHC staining, slides were baked for 1 h at 60 °C, deparaffinized with xylene (Duksan Pure Chemicals), rehydrated with sequential washes with decreasing concentrations of ethanol (Merck Millipore Corporation, Billerica, MA, USA), and rinsed with tap water (100% xylene 5 min: 2 times, xylene 1:1 with 100% ethanol 5 min: 2 times, 95% ethanol 5 min, 70% ethanol 5 min, 50% ethanol 5 min, tap water). After antigen retrieval and permeabilization, non-specific binding sites were blocked with serum-free blocking buffer (X0909; Agilent, Santa Clara, CA, USA). The slides were then incubated for overnight at 4 °C with 1:50 diluted CB_1 antibody (Cayman Chemical, Ann Arbor, MI, USA). Antibody binding was detected using a biotinylated secondary antibody and ABC reagent from the Vectastain Elite ABC kit (Vector Laboratories). The slides were developed using peroxidase substrate solution, counterstained with hematoxylin, and mounted using VectaMount mounting medium (all from Vector Laboratories). The slides were then observed and photographed with a Moticam 3.0 MP color digital camera (Motic).

To conduct ZO-1 IF staining, Caco-2 cells were seeded at a density of 1×10^4 cells/well on an eight-well chamber slide (LabTek, Thermo Fisher Scientific). After overnight stabilization, cells were treated with HU (150 μ M), SR141716A (2 μ M), and ACEA (10 μ M)

for 24 h. To detect ZO-1 in miRNA mimic- and inhibitor-transfected cells, cells were transfected during the subculture process, seeded on a chamber slide, and incubated for 48 h. After treatment, cells were fixed with 10% neutral buffered formalin solution (Sigma-Aldrich) for 30 min. Fixed cells were washed with PBS three times for 5 min each, and surface tension was reduced using 0.1% Triton X-100 for 1 h at room temperature (RT). Cells were blocked with serum-free blocking buffer (X0909, Agilent) for 1 h, incubated overnight at 4 °C in a humidified chamber with primary antibody, 5 µg/ml of ZO-1 (cat. no. 61-7300; Invitrogen Life Technologies, Gaithersburg, MD, USA). The cells were washed five times for 5 min, each with PBS containing 0.05% Tween 20. After washing, the cells were incubated for 2 h in a 1:1,000 dilution of fluorescein isothiocyanate-conjugated rabbit IgG-heavy and light chain antibody (Bethyl Laboratories, Montgomery, TX, USA). Finally, the cells were washed five times, mounted on slides with VECTASHIELD® mounting medium (Vector Laboratories, Burlingame, CA, USA), and examined with fluorescence microscopy Axioskop FL (Carl Zeiss Meditec, Inc., Dublin, CA, USA) using Metamorph Microscopy Automation and Image Analysis Software (Molecular Devices, Sunnyvale, CA, USA).

Transepithelial electrical resistance measurement

IEC-6 cells (5×10^4 cells/well) and Caco-2 cells (1×10^5 cells/well) were seeded into the upper chamber of the hanging insert (pore size, 0.4 µm, surface area, 0.33 cm², SPL Life Science, Gyeonggi-do, South Korea) of the 24-well culture plate, while the lower chamber contained the culture medium. Cell culture medium was added to both the apical chamber (200 µl) and basolateral chamber (1 ml). After 5 d, the electrical resistance of the confluent polarized IEC-6 and Caco-2 monolayers was measured by TEER using a Millicell® ERS-2 VoltOhm Meter (Merck Millipore Corporation). Both cells were used in experiments only after the TEER value had increased above 1,000 Ω/cm². IEC-6 cells were treated with H₂O₂ for 2 h and washed with fresh culture medium, with or without SR141716A and ACEA. The TEER values were measured at least five time points for 48 h, including 0 h (immediately before H₂O₂ treatment) and 2 h (immediately after H₂O₂ treatment). Caco-2 cells were treated with HU for 24 h, and at least five time points were measured for the total experimental period. SR141716A treatment was conducted at the same time as HU treatment, whereas ACEA treatment was started 30 min prior to HU treatment. The TEER values for the cell-free control wells were subtracted from the obtained values to remove background values. All TEER measurements were performed in triplicate. The relative TEER value in the transwell plates was calculated as a percentage of the TEER value at 0 h in each group, which was set to 100%.

Western blotting

Total protein was extracted from tissues and cells using a protein extraction solution (ELPIS Biotech, Daejeon, Republic of

Korea). The protein concentration of the lysates was determined using the Pierce BCA Protein Assay Kit (Thermo Fisher Scientific), according to the manufacturer's instructions. Equal amounts (20 µg) of proteins from each group were then boiled at 90 °C for 5 min in Laemmli sample buffer (ELPIS-Biotech, Daejeon, South Korea) at a volume ratio of 4:1. Total protein was separated by 10% sodium dodecyl sulfate-polyacrylamide gel electrophoresis and transferred to polyvinylidene fluoride membranes (Merck Millipore Corporation) using a wet transfer system (Hoefer Scientific, Holliston, MA, USA). The membranes were blocked with 5% skimmed milk (BD Biosciences, San Jose, CA, USA) in Tris-buffered saline with 0.05% Tween 20 (20 mM Tris, 140 mM sodium chloride, pH 7.5, and 0.05% Tween 20; Amresco, Solon, OH, USA) for 1 h at RT. The membranes were then incubated overnight at 4 °C with the primary antibodies at a 1:1,000 dilution: CB₁ (cat. no. sc-20754; Santa Cruz Biotechnology Inc., Santa Cruz, CA, USA), and p-p65 NF-κB (cat. no. 3033; Cell Signaling Technology, Inc.), and p-STAT3 (cat. no. 9131; Cell Signaling Technology, Inc.), and STAT3 (cat. no. 9132; Cell Signaling Technology, Inc.) and β-actin (cat. no.; A5441, 1:10,000, Sigma-Aldrich). After incubation, the membranes were washed five times for 10–15 min with Tris-buffered saline containing 0.05% Tween 20, and then incubated with horseradish peroxidase-conjugated anti-rabbit (cat. no. ADI-SAB-300-J), or anti-mouse (cat. no. ADI-SAB-100-J) antibody (1:10000) (both from Enzo Life Sciences, Farmingdale, NY, USA) at RT for 2 h. Antigen–antibody complexes were visualized using enhanced chemiluminescence reagents (WesternBright ECL, Advansta Corporation, San Jose, CA, USA). Densitometric analyses of protein expression were performed using ImageJ 1.47 software.

miRNA analysis and transfection

Total RNA was isolated using a Hybrid-R™ miRNA isolation kit (GeneAll Biotechnology Co. Ltd, Seoul, South Korea). To quantify miRNA transcript levels, qPCR was performed using the miRCURY LNA miRNA PCR Starter Kit (Qiagen), following the manufacturer's instructions. The primer sequences used to detect miR-191-5p and the endogenous control miR-103a-3p were as follows: hsa-miR-191-5p (5'- CAA CGG AAU CCC AAA AGC UG -3') and hsa-miR-103a-3p (5'- AGC AGC AUU GUA CAG GGC UAU GA -3').

Caco-2 cells were transfected at 70–80% confluence in a six-well plate using Lipofectamine RNAiMax (Invitrogen Life Technologies), following the manufacturer's instructions. Briefly, 25 pmol/well Lipofectamine RNAiMAX reagent was diluted in Opti-MEM medium (Gibco BRL, Gaithersburg, MD, USA), and 30 pmol/well siRNA, miRNA mimic, and inhibitor were diluted in Opti-MEM medium. Next, the diluted siRNA and diluted Lipofectamine RNAiMAX reagent were mixed in a 1:1 ratio and incubated for 5 min. A mixture of siRNA-lipid complexes was added to the cells. For miR-191a-5p regulation, 50 nmol/L of miR-191-5p mimic and inhibitor (Qiagen) and their negative controls were used (Bioneer, Daejeon, South Korea). STAT3 inhibition was achieved by transfection with 30 pmol/L STAT3 siRNA or a negative control siRNA (Bioneer). Forty-eight hours after

transfection, the cells were trypsinized, harvested, and used for experiments.

Statistical analysis

Statistical analyses were performed using GraphPad Prism version 5.03 for Windows (GraphPad Software, La Jolla, CA, USA). Data are presented as mean \pm SD. Student's *t*-test or one-way or two-way analysis of variance was used to assess statistical significance; $p < 0.05$ was considered statistically significant.

Results

CB₁ expression was decreased by aging in the small intestine

To investigate age-related changes in the expression of eCB receptors, qPCR was conducted using tissues of the small intestine

and colon from young and old rats. Interestingly, CB₁ expression was significantly decreased only in the aged small intestine (Figure 1A). In the colon, CB₁ expression did not decrease significantly (Figure 1B). The expression of CB₂ did not change in either the small intestine or the colon (Figures 1A, B). Moreover, IHC staining showed that CB₁ expression decreased in the small intestine tissues of old rats compared to those of young rats (Figures 1C, D). Histological analysis showed no significant changes in the old small intestine and colon compared to the young small intestine and colon (Figures 1E, F).

CB₁ expression was decreased by H₂O₂-induced cellular senescence

An *in vitro* model of the aged small intestine was produced by treating IEC-6 cells (a rat intestinal epithelial cell line) with H₂O₂, because H₂O₂ exposure is known to induce cellular senescence. Cell morphology of IEC-6 cells were enlarged, flattened, and irregular in shape following H₂O₂ exposure in a time-dependent manner

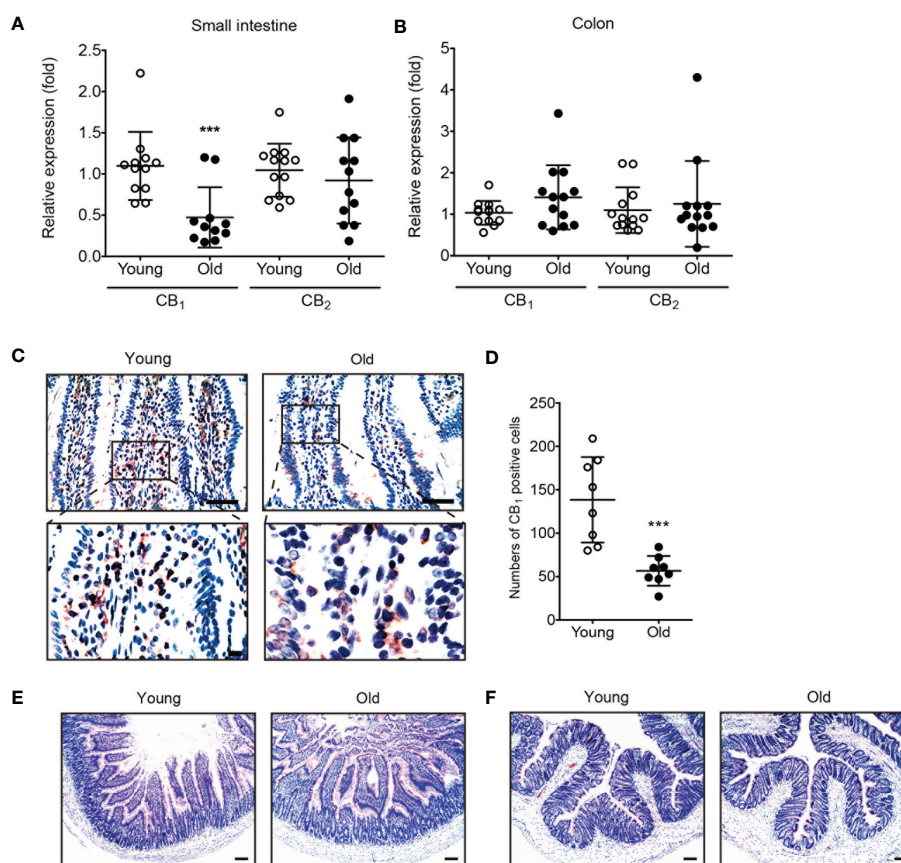


FIGURE 1

The expression of CB₁ was decreased in old rat small intestine. (A, B) qPCR was conducted to detect RNA expression levels of CB₁ and CB₂ in both young (white dot) and old (black dot) tissues of the small intestine (A) and colon (B). Statistical differences were determined using *t*-test; triple asterisks (***) indicate $p < 0.001$. Results are presented as means \pm SEMs. $n = 10$ – 12 per group. GAPDH was used for the loading control. (C) Immunohistochemistry staining was used to detect CB₁ expression in the small intestine of young and old rats. Scale bar, 50 μ m. (D) The graph shows the result of quantitative analyses by using counting of CB₁ positive cells in each phase. (***) indicate $p < 0.001$. Results are presented as means \pm SEMs. $n = 8$ per group. (E, F) Small intestine (E) and colon (F) tissue sections from young and old rats were stained with H&E. No significant change in histology was observed in either the small intestine or colon. Scale bar, 100 μ m.

(Figure 2A). We also conducted SA- β -gal staining, which is a widely used biomarker for aging cells, to confirm the β -galactosidase activity of senescent cells. H₂O₂-treated IEC-6 cells had a greater number of β -gal-positive cells than untreated cells at each time point (Figure 2B). Next, we confirmed the expression of CB₁ in the H₂O₂-treated *in vitro* aging model. The expression of CB₁ mRNA significantly decreased in H₂O₂-treated IEC-6 cells (Figure 2C). The protein levels of CB₁ were also decreased by H₂O₂ exposure in a concentration- and time-dependent manner (Figures 2D, E). Moreover, the selective CB₁ inverse agonist, SR141716A, downregulated CB₁ mRNA expression, similar to that in the H₂O₂-treated IEC-6 cells (Figure 2F). In addition, ACEA co-treatment was directly associated with increased CB₁ expression (Figure 2G). ACEA treatment successfully restored CB₁ expression after H₂O₂ treatment (Figure 2G). These results showed that CB₁ expression was decreased in an *in vitro* H₂O₂-induced cell senescence model, which is consistent with the *in vivo* aged rat tissues (Figure 1).

Increased intestinal permeability was associated with the reduction of CB₁ signaling by regulating ZO-1

To investigate whether CB₁ signaling was related to senescent cell phenotypes, we observed cell morphology and measured the TEER value after applying the agonists, SR141716A and ACEA. SR141716A treatment resulted in more aged cell morphology than the untreated control group, although it did not induce morphological changes as much as the H₂O₂ treatment (Figure 3A). The reduction in TEER value by SR141716A was as strong as that by H₂O₂ treatment, and we confirmed that both SR141716A and H₂O₂ induced approximately a 20% reduction at 24 h (Figure 3B). These results showed that the inhibition of CB₁ signaling causes intestinal epithelial cells to be considerably similar to the senescent cell phenotype induced by H₂O₂ treatment. We used ACEA to confirm whether CB₁ signaling activation can restore aged cell phenotypes and abnormally increased cell permeability. First, ACEA treatment significantly reduced the morphological alterations in H₂O₂-treated senescent cells (Figure 3C). The TEER value was significantly reduced by H₂O₂ treatment but was considerably restored by ACEA co-treatment (Figure 3D). Next, we assessed the alteration of tight junction protein levels in H₂O₂-treated IEC-6 cells. H₂O₂ treatment considerably downregulated ZO-1, ZO-2, claudin-2, claudin-4, and occludin mRNA expression (Figures 3E, F). Moreover, the cells were co-treated with ACEA, and the induction of tight junction protein expression was confirmed. Interestingly, ACEA restored the expression of ZO-1 (Figure 3G), but not that of other tight junction proteins. These results suggested that CB₁ signaling activation restores H₂O₂-induced aged cell morphology and reduces intestinal permeability by increasing the expression of tight junction proteins, especially ZO-1.

Increased intestinal permeability in HU-induced cell senescence was regulated by CB₁ signaling

Several recent studies have shown that HU can promote a senescence-like phenotype in various cell types (14–16). To establish new *in vitro* senescence models in intestinal cells, Caco-2 human colonic epithelial adenocarcinoma cells were treated with HU. HU treatment induced senescent cell morphology (Figure 4A) and increased β -gal staining intensity (Figure 4B). Both the mRNA and protein expression levels of the CB₁ were significantly decreased in HU-induced Caco-2 cells (Figures 4C, D). To confirm whether the regulation of CB₁ signaling in HU-induced aged cells is similar to that in H₂O₂-induced aged cells, SR141716A and ACEA were used to treat HU-induced aged Caco-2 cells. Inhibition of CB₁ signaling by SR141716A resulted in considerably aged cell phenotypes (Figure 4E, top), and increased β -gal-positive cells similar to HU-induced aged cells (Figure 4E, bottom). SR141716A treatment significantly decreased CB₁ expression compared to the untreated control, and the decreased level of expression was similar to HU treatment of Caco-2 cells (Figure 4F). The TEER value was significantly lower in both HU- and SR141716A-treated Caco-2 cells than that in non-treated control cells (Figure 4G). Moreover, the intensity of IF staining for ZO-1 in tight junctions was clearly diminished in both HU- and SR141716A-treated Caco-2 cells compared to that for ZO-1 in non-treated control cells (Figure 4H). Meanwhile, the activation of CB₁ signaling by co-treatment with ACEA for 6 d after pretreatment for 30 min showed protective effects against HU-induced cell senescence. The ACEA co-treatment group with HU-induced aging cells had a less flattened morphology and slightly decreased β -gal-positive cells compared to HU-induced aging cells (Figure 4I). The decreased CB₁ protein expression after HU treatment was significantly restored by ACEA co-treatment (Figure 4J). The TEER value was also increased and normalized by ACEA co-treatment compared to the HU-treated group (Figure 4K). Continuous linear staining of ZO-1 was considerably decreased by HU treatment; however, ACEA co-treatment remarkably restored the intensity of ZO-1 staining (Figure 4L). These results suggested that the increase in intestinal permeability caused by HU-induced cell senescence is tightly regulated by CB₁ signaling.

miR-191-5p regulated intestinal permeability by targeting ZO-1

To identify putative miRNAs, we employed two different computational programs: miRDB (<http://mirdb.org>) and TargetScan Human Release 8.0 (<https://www.targetscan.org>), to predict miRNAs containing targeting sites for ZO-1 mRNA. miR-191-5p showed a remarkably high prediction scores in both algorithms, with 88 and 97 points in the miRDB and TargetScan, respectively. These *in silico* analyses revealed that miR-191-5p

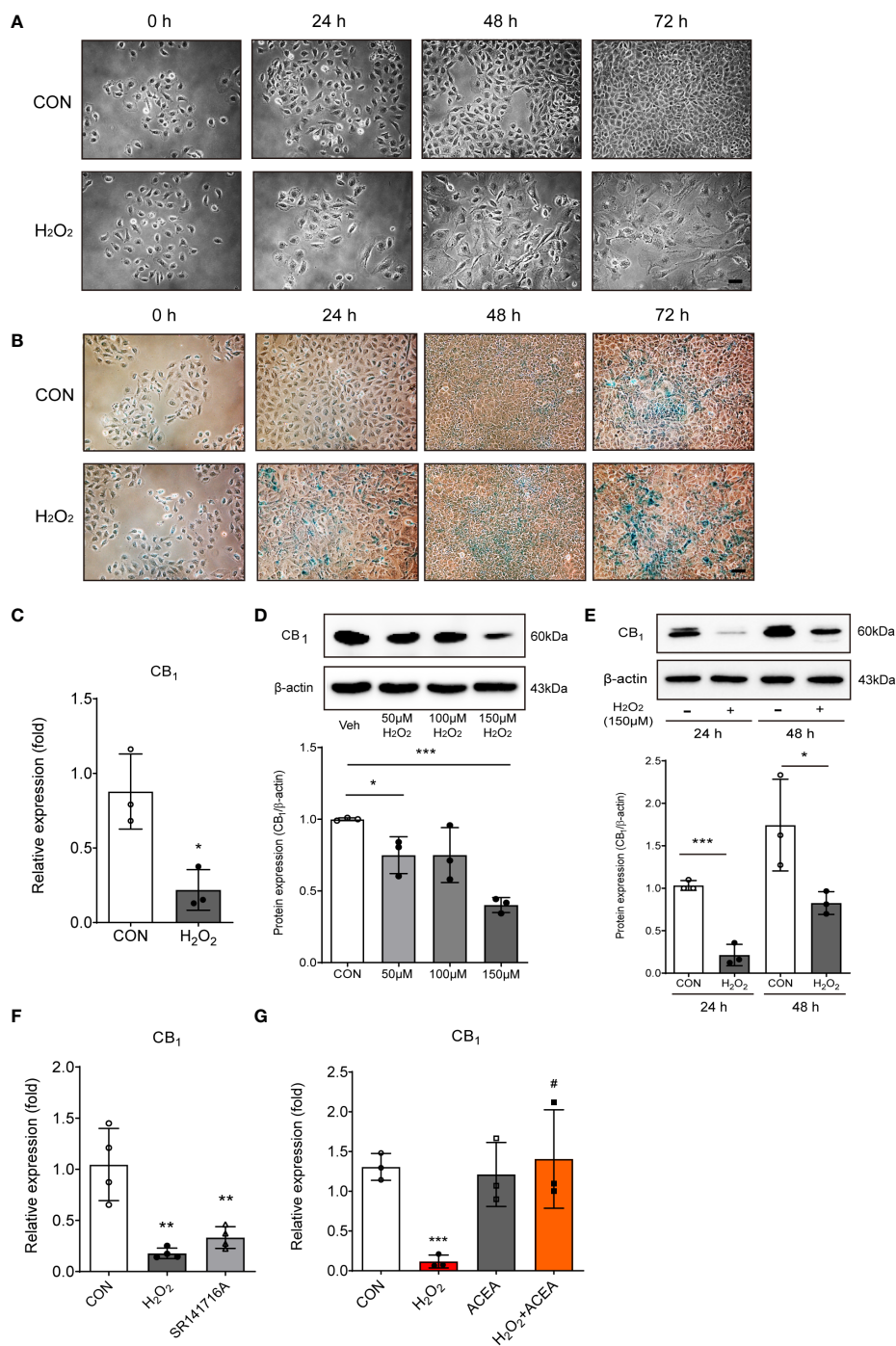


FIGURE 2

H₂O₂-induced cell senescence *in vitro* model induced CB₁ reduction. **(A)** Morphological changes showed IEC-6 cell senescence by H₂O₂ treatment (150 μM) in a time-dependent manner (n=3). Scale bar, 100 μm. **(B)** β-gal staining indicated that positive cells (blue) increased with H₂O₂ treatment (150 μM) in a time-dependent manner (n=5). Scale bar, 100 μm. **(C)** qPCR was conducted to confirm the RNA expression of CB₁ in H₂O₂-treated IEC-6 cells. Statistical differences were determined using *t*-test; a single asterisk (*) indicates *p*<0.05 compared to the control group. Error bars, SD (n=3). GAPDH was used for the loading control. **(D, E)** Western blot analysis was conducted to investigate the CB₁ expression alteration by H₂O₂ treatment. The bar graphs represent the optical density quantification of the protein bands for each group **(D, E, bottom)**. Statistical differences were determined using *t*-test; a single asterisk (*) indicates *p*<0.05, triple asterisks (***) indicate *p*<0.001 compared to control group. Error bars, SD (n=3). β-actin was used for the loading control. **(F, G)** CB₁ mRNA expression was detected by qPCR in H₂O₂-treated IEC-6 cells and in cells treated with the selective CB₁ inverse agonist, SR141716A **(F)**, and/or the selective CB₁ agonist ACEA **(G)**. Statistical differences were determined using *t*-test; ***p*<0.01 and ****p*<0.001 compared to control group. #*p*<0.05 compared to H₂O₂-treated group. Error bars, SD (n=3).

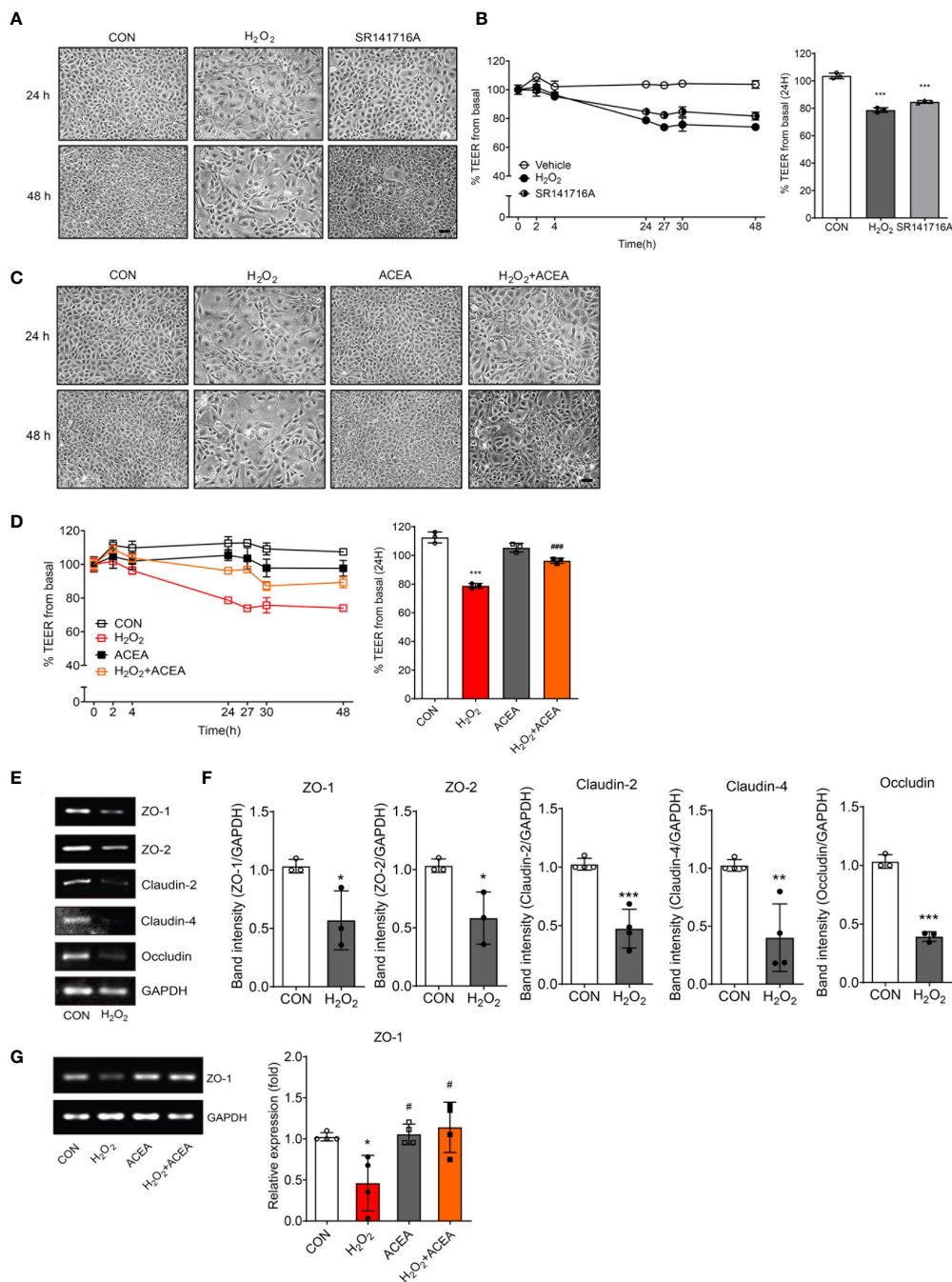


FIGURE 3

Intestinal permeability and tight junction protein expression were regulated by CB₁ signaling modulation. **(A)** Morphological changes showed IEC-6 cell senescence by H₂O₂ and SR141716A treatment (n=5). Scale bar, 100 μm. **(B)** The TEER values were detected in H₂O₂-treated IEC-6 cells and cells treated with the CB₁ inverse agonist SR141716A. The bar graph indicated the TEER values at 24 h **(B, right)**. Statistical differences were determined using *t*-test; ****p*<0.001 compared to control group. Error bars, SD (n=3). **(C)** Morphological changes showed IEC-6 cell senescence caused by H₂O₂ and the restoration of cell morphology with ACEA treatment after 24 h and 48 h (n=5). Scale bar, 100 μm. **(D)** The decreased TEER values caused by H₂O₂ treatment were increased by co-treatment with the CB₁ agonist ACEA. The bar graph presents the TEER values at 24 h after treatment with H₂O₂ and ACEA **(D, right)**. Statistical differences were determined using *t*-test; ****p*<0.001 compared to control group and ###*p*<0.001 compared to H₂O₂-treated group. Error bars, SD (n=3). **(E, F)** The mRNA expression levels of the tight junction proteins ZO-1, ZO-2, Claudin-2, Claudin-4 and Occludin were detected by RT-PCR in H₂O₂-treated IEC-6 cells. RT-PCR results showed a decrease in the levels of these tight junction proteins **(E)** and the bar graph presents the band intensity of the RT-PCR results **(F)**. Statistical differences were determined using *t*-test; **p*<0.05, ***p*<0.01, and ****p*<0.001 compared to control group. Error bars, SD (n = 3). GAPDH was used for the loading control. **(G)** Decreased RNA expression of ZO-1 by H₂O₂ was restored by ACEA co-treatment. The bar graphs present the band intensity of PCR results. Statistical differences were determined using *t*-test; **p*<0.05 compared to control group and #*p*<0.05 compared to H₂O₂-treated group. Error bars, SD (n = 3).

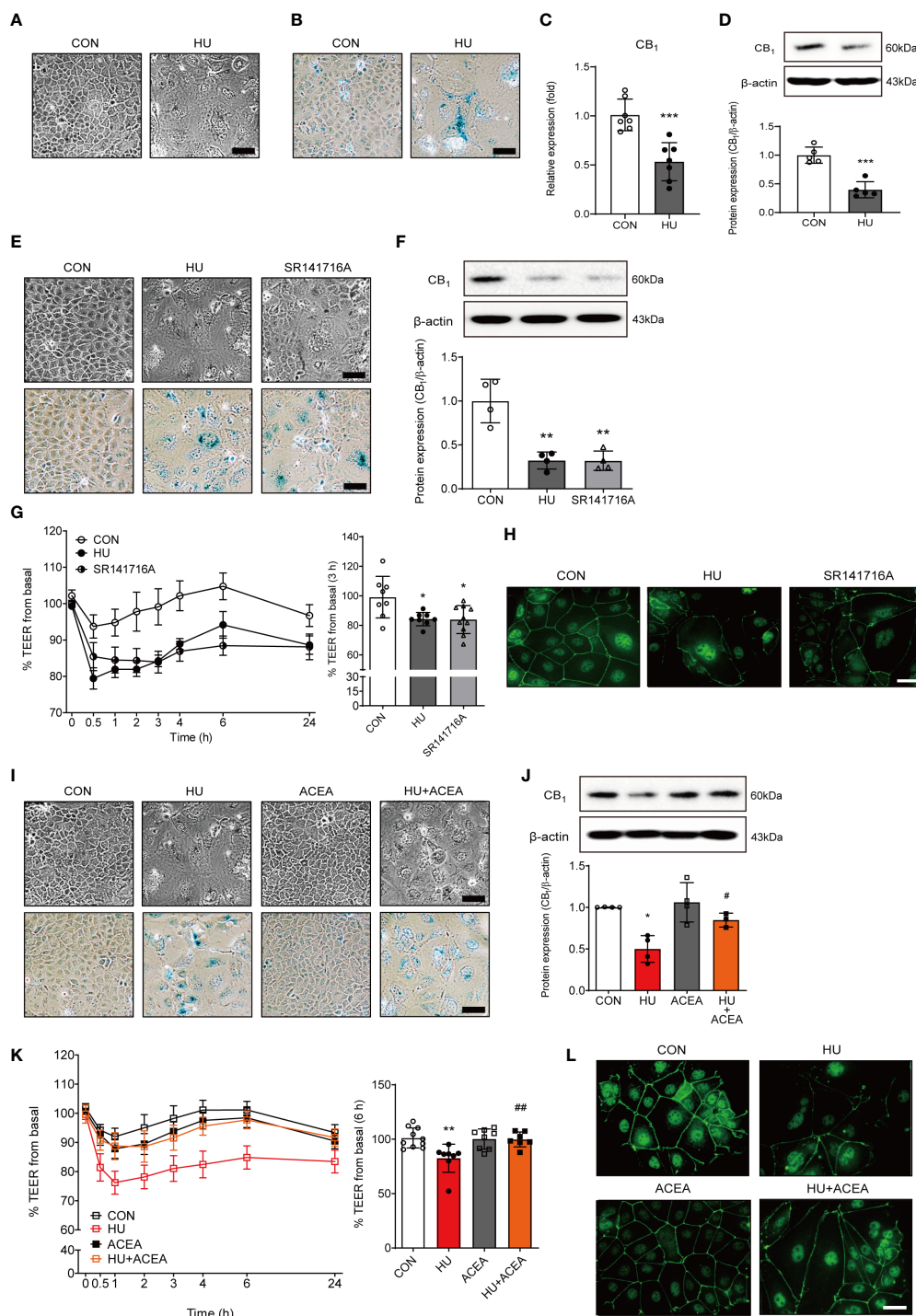


FIGURE 4

The characteristics of cell senescence and alteration of the TEER value and ZO-1 expression are regulated by CB₁ signaling. **(A, B)** HU treatment induced morphological changes **(A)** and positive cell intensity in β-gal staining **(B)** in Caco-2 cells. Scale bar, 50 μm. **(C, D)** The alteration of CB₁ expression was detected by qPCR **(C)** and western blot **(D)**. The bar graph presents the optical density quantification of the protein bands for each group **(D, bottom)**. Statistical differences were determined using *t*-test; ****p*<0.001 compared to control group. Error bars, SD (n = 3). **(E)** Cell morphology **(E, upper)** and β-gal staining **(E, bottom)** were determined in HU-induced aged cells and SR141716A-treated Caco-2 cells. Scale bar, 50 μm. **(F)** Representative bands from western blot and quantitative analyses of CB₁ protein expression in Caco-2 cells after HU and SR141716A treatment are shown. β-actin was used as a loading control. Error bars, SD (n = 3). ***p*<0.01 vs. the control group. **(G)** The effects of HU and SR141716A on Caco-2 cell permeability. Continual resistance values of the Caco-2 cell monolayers are shown. The bar graph presents the TEER values at 3 h after treatment with HU and SR141716A **(G, right)**. Statistical differences were determined using *t*-test; **p*<0.05 compared to control group. Error bars, SD (n = 8). **(H)** Representative pictures of IF staining of ZO-1 in Caco-2 cells treated with HU and SR141716A. Scale bar, 50 μm. **(I)** Cell morphology **(I, upper)** and β-gal staining **(I, bottom)** in HU-induced aged cells and/or ACEA-treated Caco-2 cells. Scale bar, 50 μm. **(J)** Representative bands of western blot and quantitative analyses of CB₁ protein expression in Caco-2 cells after HU and/or ACEA treatment are shown. β-actin was used as a loading control. Error bars, SD (n = 3). **p*<0.05 compared to control group, #*p*<0.05 compared to HU treatment group. **(K)** The effects of HU and/or ACEA on Caco-2 cell permeability. Continual resistance values of the Caco-2 cell monolayers are shown. The bar graph presents the TEER values at 6 h after treatment with HU and/or ACEA **(K, right)**. Statistical differences were determined using *t*-test; ***p*<0.01 compared to control group, ##*p*<0.01 compared to HU treatment group. Error bars, SD (n = 8). **(L)** Representative pictures of IF staining of ZO-1 in Caco-2 cells treated with HU and/or ACEA. Scale bar, 50 μm.

directly targeted ZO-1 mRNA to inhibit its translation. The 297-304 position in the 3' UTR of ZO-1 mRNA contained a putative binding site, which is a completely complementary sequence of the seed region of miR-191-5p (Figure 5A). Both HU-induced cell senescence and inhibition of CB₁ signaling by SR141716A significantly increased the expression of miR-191-5p (Figure 5B). ACEA co-treatment considerably decreased the expression of HU-induced miR-191-5p (Figure 5C). Next, to investigate the functions

of miR-191-5p in intestinal permeability, we used an miR-191-5p mimic and inhibitor. Transfection of the miR-191-5p mimic and inhibitor successfully overexpressed and inhibited miR-191-5p expression, respectively (Figures 5D, E). Overexpression of miR-191-5p by mimic transfection decreased TEER value and ZO-1 expression (Figures 5F, G). In contrast, transfection with the miR-191-5p inhibitor increased the TEER value and ZO-1 expression (Figures 5H, I). These results indicated that miR-191-5p is involved

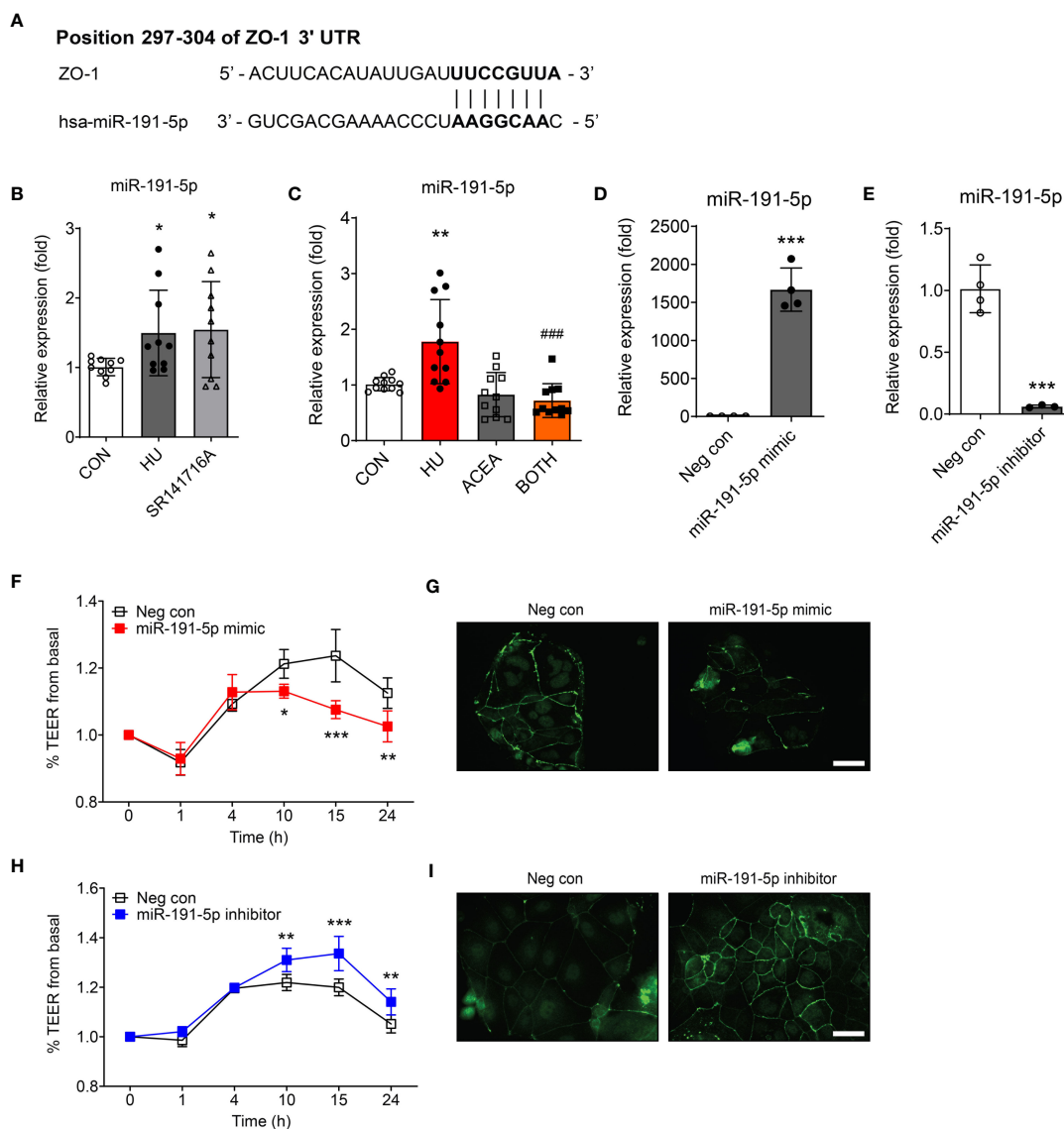


FIGURE 5

Intestinal permeability was regulated by miR-191-5p targeting ZO-1. (A) The likelihood of miRNA targeting ZO-1 was predicted using two independent miRNA target databases. It showed 7–8 mer sequences (black bold) of miR-191-5p binding positions within 3' UTR of ZO-1 mRNA. (B, C) qPCR was used to compare the alteration of miR-191-5p expression after SR141716A (B) and ACEA treatments (C) to that in the HU-treated aged Caco-2 cells. miR-103a-3p was used as a loading control. Error bars, SD (n = 3). *p<0.05, **p<0.01 vs. the control group, ###p<0.001 vs. the HU treatment group. (D, E) The transfection efficacy of miR-191-5p mimic (D) and inhibitor (E) were tested by qPCR for miR-191-5p expression. Error bars, SD (n = 3). ***p<0.001 vs. the negative control group. (F–I) The TEER values were measured to investigate the change of intestinal permeability in Caco-2 cell monolayer by transfection of miR-191-5p mimic (F) and inhibitor (H). Statistical differences were determined using two-way ANOVA; *p<0.05, **p<0.01, ***p<0.001 vs. the negative control group. Error bars, SD (n = 4). IF staining of ZO-1 was also conducted, and representative pictures were selected of Caco-2 cells transfected with miR-191-5p mimic (G) and inhibitor (I). Scale bar, 50 μm.

in the regulation of intestinal permeability in HU-induced senescent cells by targeting ZO-1.

Phosphorylation of NF- κ B p65 is tightly regulated by CB₁/miR-191-5p-related signaling in HU-induced aged cells

Previous reports have showed that the transcriptional regulation of ZO-1-mediated barrier permeability is related to NF- κ B signaling and STAT3 signaling (17–19). Also, miR-191 is closely linked to the activation of pro-inflammatory pathways, such

as NF- κ B signaling (18). To determine the specific miR-191-5p-related molecular regulator upstream of ZO-1, we tested the changes in NF- κ B and STAT3 signaling. The phosphorylation of NF- κ B p65 was increased and phosphorylation of STAT3 was decreased in HU-induced aged Caco-2 cells, but activation of the CB₁ by ACEA co-treatment successfully restored these alterations of phosphorylation (Figures 6A, D). Transfection of Caco-2 cells with the miR-191-5p mimic increased the phosphorylation of NF- κ B p65 (Figure 6B), whereas miR-191-5p inhibitor transfection inhibited the phosphorylation of NF- κ B p65 (Figure 6C). However, phosphorylation of STAT3 did not show any significant changes in either miR-191-5p mimic- or inhibitor-transfected Caco-2 cells

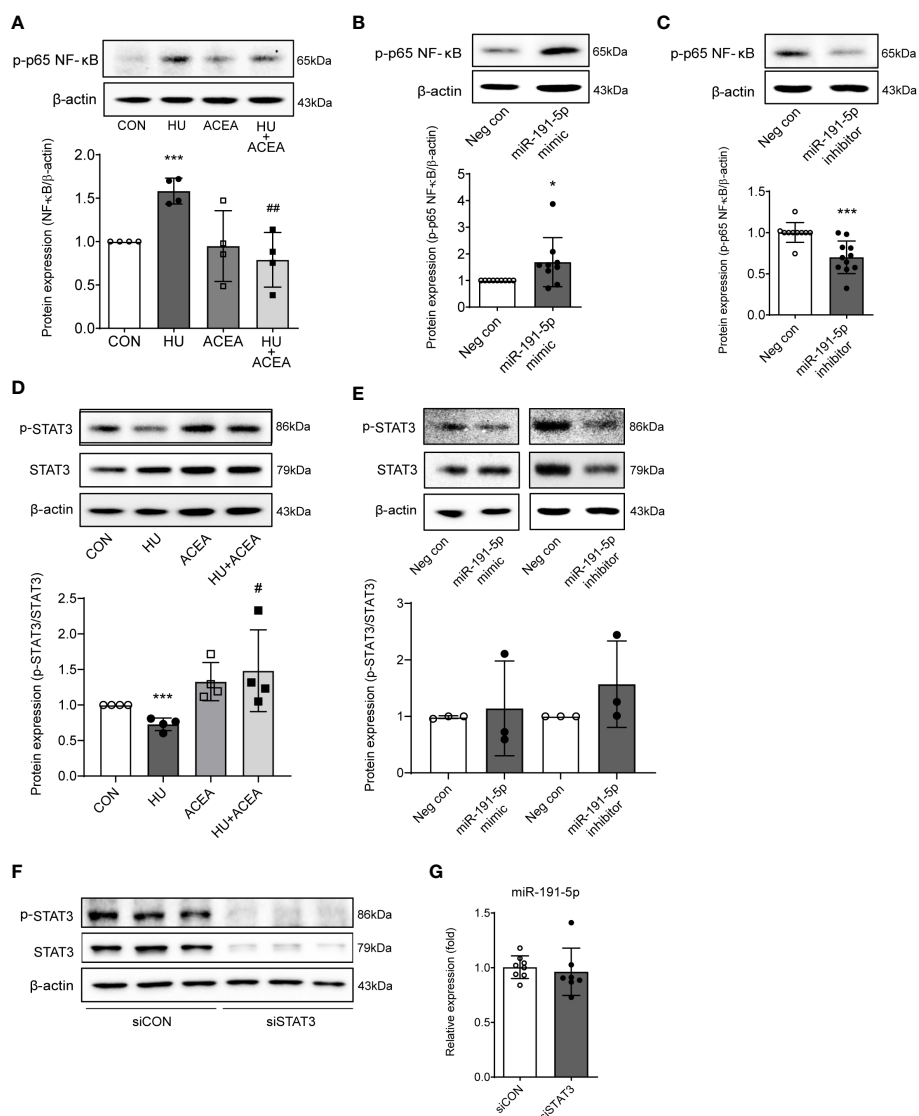


FIGURE 6

Phosphorylation of NF- κ B p65 was modulated by miR-191-5p in HU-induced cell senescence. (A, D) Representative bands of western blot and quantitative analyses of phosphorylation of NF- κ B p65 (A) and p-STAT3 (D) protein expression levels in Caco-2 cells after HU and/or ACEA treatment are shown. Error bars, SD (n = 3). ***p<0.001 compared to control group, #p<0.05, ##p<0.01 compared to HU treatment group. (B, C) The protein expression level of NF- κ B p65 phosphorylation was detected by western blot in miR-191-5p mimic- (B) and inhibitor- (C) transfected Caco-2 cells. Error bars, SD (n = 3). *p<0.05, ***p<0.001 compared to negative control group. (E) Phosphorylation of STAT3 was evaluated with miR-191-5p mimic- and inhibitor-transfected Caco-2 cells. The bar graph below shows the result of quantitative analysis. (F) p-STAT and STAT3 protein expression was shown in cells transiently transfected with siRNA of STAT3. (G) miR-191-5p expression in transiently transfected Caco-2 cells with siSTAT3 was measured using qPCR. Error bars, SD (n = 3).

(Figure 6E). Moreover, the expression of miR-191-5p did not change upon STAT3 knockdown by siSTAT3-transfection in Caco-2 cells (Figures 6F, G). These results implied that NF- κ B p65 activation is directly regulated by miR-191-5p, but STAT3 signaling is independent of miR-191-5p, even though it is involved in the CB₁ signaling pathway during cell senescence.

Discussion

Increased intestinal tight junction permeability in the aging gut is a well-known physiological change, but the reason for this is not yet fully understood. This is the first report indicating that CB₁ signaling is directly related to aging gut permeability through the downregulation of ZO-1 protein. Our results also demonstrated the detailed mechanisms by which miR-191-5p and NF- κ B p65 activation are closely associated with intestinal permeability by the downregulation of ZO-1 in CB₁ defected aging gut (Figure 7).

Our results showed that the expression of the CB₁ was significantly decreased in the small intestine of old rats compared to that of young rats (Figure 1A). To create an *in vitro* model of the aged intestinal epithelium, the expression of CB₁ was also significantly decreased by H₂O₂ and HU treatment compared to the vehicle-treated control in both concentration- and time-dependent manners (Figures 2, 4). Our results are consistent with those of a previous study that showed a reduction in CB₁ expression in aged human brain tissues (10). The specific reasons and mechanisms underlying the decline in CB₁ expression during aging remain unknown. One possibility is that the decline in CB₁

expression is accompanied with alteration in the levels of cannabinoid ligands because it is synthesized and released “on demand” (20). Therefore, decreased levels of endogenous cannabinoid ligands, as well as increased levels of its catabolizing enzymes, can cause a decrease in signaling of the cannabinoid system during aging (20, 21). Previous reports have indicated that CB₁ exert protective effects against increased intestinal motility and epithelial damage during intestinal inflammation (7). As aging progresses, the expression of the CB₁ gradually declines, diminishing its protective effect in the gut.

In contrast, the expression level of the CB₂ showed no significant change with aging (Figures 1A, B). The CB₂ is generally expressed in immune cells, such as macrophages and plasma cells, and is highly associated with inflammation (22). Additionally, the CB₂ expression is upregulated in the colonic epithelium of patients with inflammatory bowel disease, and it may exert anti-inflammatory effects (23). Therefore, CB₂ expression may contribute to the regulation of abnormal inflammatory pathogenesis, rather than age-related intestinal physiology. Although further studies are required to investigate more specific functions and characterizations of the eCB system in the aging gut, this is meaningful as the first report to show that alterations in CB₁ and CB₂ expression levels in the intestine reflect age-associated changes.

In elderly people, abnormal intestinal permeability, also known as a leaky gut, may be a causative factor driving chronic and difficult-to-treat health problems, and elderly people have been shown to be at greater risk for the development of autoimmune disorders than younger adults (2). Endogenous cannabinoids have

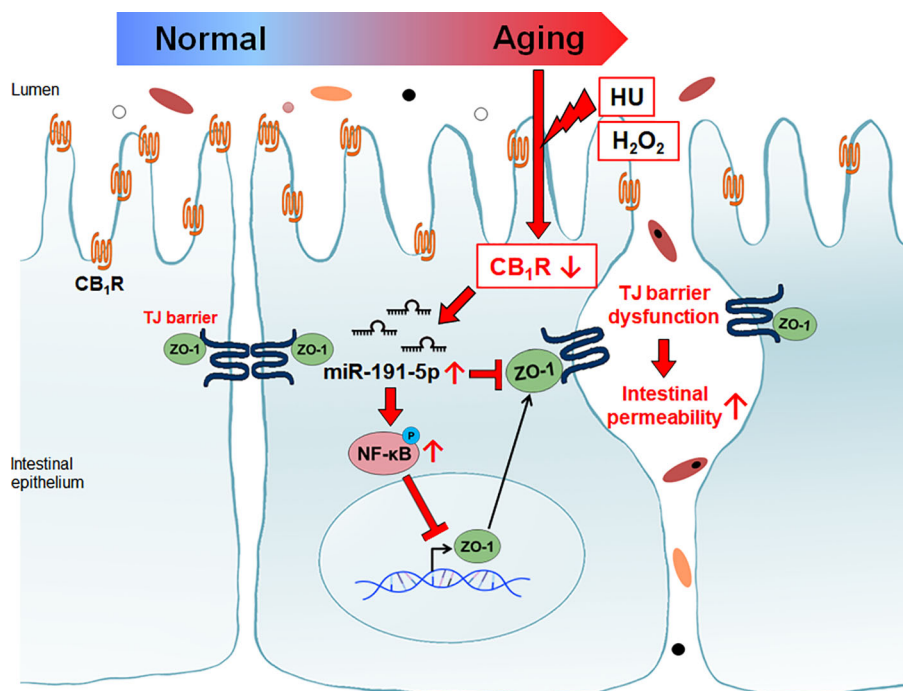


FIGURE 7

Reduction of CB₁ in aged intestinal epithelial cells caused tight junction dysfunction. Decreased CB₁ is associated with the induction of miR-191-5p. miR-191-5p reduced ZO-1 expression by targeting directly and via activation of p-p65 NF- κ B transcription factor.

the ability to increase permeability, resulting in inflammation, whereas exogenous phytocannabinoids can inhibit or recover cytokine-induced increased permeability (24). Plant-derived synthetic cannabinoids also reduce abnormal intestinal permeability, suggesting their therapeutic potential (8). In murine colitis, cannabinoids decrease histologic and microscopic inflammation (25). Although many studies have discussed the regulation of intestinal permeability through the activation of CB receptors by exogenous or endogenous cannabinoids, there is no evidence regarding the association between age-related intestinal permeability and the eCB system.

In our results, an *in vitro* model of aged intestinal epithelium demonstrated a reversible decrease in TEER (i.e., increased intestinal permeability) over the measurement period. The recovery of morphological changes in cell senescence, as well as TEER values of H₂O₂ and HU treatments, was demonstrated by treatment with the CB₁ selective agonist ACEA (Figures 3C, D, 4I, K). Moreover, treatment with the ACEA upregulated the HU-induced decrease in CB₁ expression (Figure 4J). Our data suggested that increased intestinal permeability in the aging gut is highly associated with decreased expression levels of the CB₁ and inhibition of CB₁ signaling. Moreover, reactivation of CB₁ signaling successfully restored intestinal permeability. These results provide new information regarding the close relationship between CB₁ signaling and abnormally increased intestinal permeability in the aging gut.

Meanwhile, SR141716A treatment decreased CB₁ expression to the same extent as HU treatment (Figure 4F). Originally, SR141716A was well-described as an antagonist of CB₁, but it exerts inverse agonist activity by conformational stabilization of the inactive state of CB₁ (26). The inverse agonist activity of SR141716A directly inhibits the activation of peripheral CB₁ (27). In our study, SR141716A directly reduced CB₁ expression without other stimulation. Additionally, the inverse agonism of SR141716A reduced CB₁ activity, consequently showing similar phenotypes to senescence-induced cells. SR141716A treatment mimicked cell senescence and increased intestinal permeability (Figures 3A, B, 4E, G).

In the regulation of gut barrier function, the eCB system plays an important role as a control tower for gut permeability by altering the distribution of tight junction proteins (28, 29). In our screening data, H₂O₂-treated aged IEC-6 showed significantly decreased levels of most tight junction proteins, including ZO-1, ZO-2, claudin-2, claudin-4, and occludin, compared to non-treated vehicle controls (Figures 3E, F). Furthermore, activation of CB₁ signaling by co-treatment with ACEA restored the expression of ZO-1 but not that of other tight junction proteins (Figure 3G). In Caco-2 cells, the intensity of IF staining for ZO-1 markedly decreased HU- and SR141716A-treated cells, and co-treatment with ACEA resulted in a slight increase in the expression of ZO-1 (Figures 4H, L). These results suggested that ZO-1 plays an important role in regulating CB₁-related intestinal permeability in the aging gut.

As the last step, we investigated the underlying molecular mechanisms of ZO-1 tight junction proteins in aged intestinal epithelium using miRNA analysis. Some studies have demonstrated that miRNAs are extensively involved in the ZO-1-

associated intestinal epithelial barrier function. For example, miR-155 is overexpressed in the intestinal epithelia of severe acute pancreatitis, consequently inhibiting the synthesis of ZO-1 and E-cadherin (30). Overexpression of miR-21 is associated with an impaired intestinal epithelial barrier and decreased ZO-1 and occludin expression levels (31). However, these miRNAs indirectly downregulate ZO-1 by targeting the Rho family of GTPases, such as RhoA and RhoB (30, 31). For this reason, we aimed to find the optimal miRNA satisfying two requirements: 1) targeting ZO-1 directly; 2) associating CB₁ signaling. Finally, we selected miR-191-5p as a novel CB₁ signaling-associated miRNA targeting ZO-1. According to a previous study, miR-191-5p accelerates TNF- α -induced intestinal epithelial injury by ZO-1 depletion in IEC-6 cells (32). Similarly, miR-191-5p activation inhibited ZO-1 expression and decreased the TEER value, suggesting an increase in intestinal permeability in Caco-2 cells (Figures 5F, G). Inhibition of miR-191-5p showed the opposite results by increasing ZO-1 expression and TEER value (Figure 5H, I). Moreover, the expression of miR-191-5p was increased in HU- and SR141716A-treated senescent Caco-2 cells and decreased in ACEA-co-treated HU-induced aged Caco-2 cells (Figures 5B, C). These results indicated that miR-191-5p is highly associated with CB₁ signaling in senescence-induced cells, suggesting that the regulation of the CB₁ in aging-induced intestinal permeability is involved in miR-191-5p-dependent signaling.

In conclusion, our data indicated that the reduction of CB₁ in H₂O₂- and HU-treated aging cells causes the induction of miR-191-5p expression, increased NF- κ B p65 phosphorylation, decreased ZO-1 expression, and functional opening of the intestinal tight junction barrier. Therefore, our results implied that modulation of the eCB system is important for the regulation of aging-associated intestinal permeability and inflammation. Understanding the aging gut physiology is important for maintaining healthy conditions in the aged population. This study provides clues for the development of therapeutic adaptation by activating the CB₁ to treat intestinal disorders in the elderly population. Returning and restoring eCB system homeostasis in the aging gut is essential for improving the quality of life in elderly population.

Data availability statement

The original contributions presented in the study are included in the article/supplementary materials, further inquiries can be directed to the corresponding author.

Ethics statement

The animal study was approved by Institutional Animal Care Committee of the Pusan National University (Approval Number PNU-2012-0088). The study was conducted in accordance with the local legislation and institutional requirements.

Author contributions

YL performed the experiments, analyzed the data and wrote the manuscript. YK, SP, and GH performed the experiments. HC contributed the rat samples and interpreted the data. EI conceived the idea, designed the research, interpreted the data, and wrote the manuscript. All authors contributed to the article and approved the submitted version.

Funding

This work was supported by the National Research Foundation of Korea (NRF) grant funded by the Korea government (MSIT) (No. NRF-2022R1A2C1012377 to EI) and by Basic Science Research Program through the National Research Foundation of Korea (NRF) funded by the Ministry of Education (No. NRF-2021R1A6A3A01087379 to YL).

References

- Saffrey MJ. Aging of the mammalian gastrointestinal tract: a complex organ system. *Age (Dordr)* (2014) 36:9603. doi: 10.1007/s11357-013-9603-2
- Karper WB. Intestinal permeability, moderate exercise, and older adult health. *Holistic Nurs practice*. (2011) 25:45–8. doi: 10.1097/HNP.0b013e3181fe26ff
- Maynard CL, Elson CO, Hatton RD, Weaver CT. Reciprocal interactions of the intestinal microbiota and immune system. *Nature* (2012) 489:231–41. doi: 10.1038/nature11551
- Nicoletti C. Age-associated changes of the intestinal epithelial barrier: local and systemic implications. *Expert Rev Gastroenterol Hepatol* (2015) 9:1467–9. doi: 10.1586/17474124.2015.1092872
- Ulluwishewa D, Anderson RC, McNabb WC, Moughan PJ, Wells JM, Roy NC. Regulation of tight junction permeability by intestinal bacteria and dietary components. *J Nutr* (2011) 141:769–76. doi: 10.3945/jn.110.135657
- Tran L, Greenwood-Van Meerveld B. Age-associated remodeling of the intestinal epithelial barrier. *J Gerontol A Biol Sci Med Sci* (2013) 68:1045–56. doi: 10.1093/geronol/glt106
- Lee Y, Jo J, Chung HY, Pothoulakis C, Im E. Endocannabinoids in the gastrointestinal tract. *Am J Physiol Gastrointestinal liver Physiol* (2016) 311:G655–G666. doi: 10.1152/ajpgi.00294.2015
- Alhamoruni A, Lee AC, Wright KL, Larvin M, O'Sullivan SE. Pharmacological effects of cannabinoids on the Caco-2 cell culture model of intestinal permeability. *J Pharmacol Exp Ther* (2010) 335:92–102. doi: 10.1124/jpet.110.168237
- Berrendero F, Romero J, Garcia-Gil L, Suarez I, de la Cruz P, Ramos JA, et al. Changes in cannabinoid receptor binding and mRNA levels in several brain regions of aged rats. *Bba-Mol Basis Dis* (1998) 1407:205–14. doi: 10.1016/S0925-4439(98)00042-8
- Glass M, Dragunow M, Faull RL. Cannabinoid receptors in the human brain: a detailed anatomical and quantitative autoradiographic study in the fetal, neonatal and adult human brain. *Neuroscience* (1997) 77:299–318. doi: 10.1016/s0306-4522(96)00428-9
- Wang L, Liu J, Harvey-White J, Zimmer A, Kunos G. Endocannabinoid signaling via cannabinoid receptor 1 is involved in ethanol preference and its age-dependent decline in mice. *Proc Natl Acad Sci United States America*. (2003) 100:1393–8. doi: 10.1073/pnas.0336351100
- Bilkei-Gorzo A, Racz I, Valverde O, Otto M, Michel K, Sastre M, et al. Early age-related cognitive impairment in mice lacking cannabinoid CB1 receptors. *Proc Natl Acad Sci United States America*. (2005) 102:15670–5. doi: 10.1073/pnas.0504640102
- Bilkei-Gorzo A, Drews E, Albayram O, Piyanova A, Gaffal E, Tueting T, et al. Early onset of aging-like changes is restricted to cognitive abilities and skin structure in Cnr1(-)/(-) mice. *Neurobiol aging* (2012) 33:200.e11–22. doi: 10.1016/j.neurobiolaging.2010.07.009

Acknowledgments

The authors thank the Korean Aging Tissue Bank (Busan, Korea) for providing research materials and information.

Conflict of interest

The authors declare that the research was conducted in the absence of any commercial or financial relationships that could be construed as a potential conflict of interest.

Publisher's note

All claims expressed in this article are solely those of the authors and do not necessarily represent those of their affiliated organizations, or those of the publisher, the editors and the reviewers. Any product that may be evaluated in this article, or claim that may be made by its manufacturer, is not guaranteed or endorsed by the publisher.

- Yu Q, Cheng X. Hydroxyurea-induced membrane fluidity decreasing as a characterization of neuronal membrane aging in Alzheimer's disease. *Aging (Albany NY)* (2021) 13:12817–32. doi: 10.18632/aging.202949
- Kapor S, Čokić V, Santibanez JF. Mechanisms of hydroxyurea-induced cellular senescence: an oxidative stress connection? *Oxid Med Cell Longev* (2021) 2021:7753857. doi: 10.1155/2021/7753857
- Guo Y, Tang Z, Yan B, Yin H, Tai S, Peng J, et al. PCSK9 (Proprotein convertase subtilisin/kexin type 9) triggers vascular smooth muscle cell senescence and apoptosis: implication of its direct role in degenerative vascular disease. *Arterioscler Thromb Vasc Biol* (2022) 42:67–86. doi: 10.1161/atvbaha.121.316902
- Fang Y, Wu C, Wang Q, Tang J. Farnesol contributes to intestinal epithelial barrier function by enhancing tight junctions via the JAK/STAT3 signaling pathway in differentiated Caco-2 cells. *J Bioenerg Biomembr* (2019) 51:403–12. doi: 10.1007/s10863-019-09817-4
- Gu Y, Ampofo E, Menger MD, Laschke MW. miR-191 suppresses angiogenesis by activation of NF-κB signaling. *FASEB J Off Publ Fed Am Societies Exp Biol* (2017) 31:3321–33. doi: 10.1096/fj.201601263R
- Zhou H, Jin C, Cui L, Xing H, Liu J, Liao W, et al. HMGB1 contributes to the irradiation-induced endothelial barrier injury through receptor for advanced glycation endproducts (RAGE). *J Cell Physiol* (2018) 233:6714–21. doi: 10.1002/jcp.26341
- Tao R, Li C, Jaffe AE, Shin JH, Deep-Soboslay A, Yamin R, et al. Cannabinoid receptor CNR1 expression and DNA methylation in human prefrontal cortex, hippocampus and caudate in brain development and schizophrenia. *Transl Psychiatry* (2020) 10:158. doi: 10.1038/s41398-020-0832-8
- Li R, Huang Z, Luo J, Luo H, Wang W. Downregulation of the CB1-mediated endocannabinoid signaling underlies D-galactose-induced memory impairment. *Front Mol Neurosci* (2020) 13:130. doi: 10.3389/fnmol.2020.00130
- Wright K, Rooney N, Feeney M, Tate J, Robertson D, Welham M, et al. Differential expression of cannabinoid receptors in the human colon: cannabinoids promote epithelial wound healing. *Gastroenterology* (2005) 129:437–53. doi: 10.1016/j.gastro.2005.05.026
- Izzo AA. The cannabinoid CB(2) receptor: a good friend in the gut. *Neurogastroenterol Motil*. (2007) 19:704–8. doi: 10.1111/j.1365-2982.2007.00977.x
- Alhamoruni A, Wright KL, Larvin M, O'Sullivan SE. Cannabinoids mediate opposing effects on inflammation-induced intestinal permeability. *Br J Pharmacol* (2012) 165:2598–610. doi: 10.1111/j.1476-5381.2011.01589.x
- Feng YJ, Li YY, Lin XH, Li K, Cao MH. Anti-inflammatory effect of cannabinoid agonist WIN55, 212 on mouse experimental colitis is related to inhibition of p38MAPK. *World J Gastroenterol WJG* (2016) 22:9515–24. doi: 10.3748/wjg.v22.i43.9515

26. Shim JY, Bertalovitz AC, Kendall DA. Probing the interaction of SR141716A with the CB1 receptor. *J Biol Chem* (2012) 287:38741–54. doi: 10.1074/jbc.M112.390955
27. Gross A, Terraza A, Marchant J, Bouaboula M, Ouahrani-Bettache S, Liautard JP, et al. A beneficial aspect of a CB1 cannabinoid receptor antagonist: SR141716A is a potent inhibitor of macrophage infection by the intracellular pathogen *Brucella suis*. *J leukocyte Biol* (2000) 67:335–44. doi: 10.1002/jlb.67.3.335
28. Everard A, Cani PD. Diabetes, obesity and gut microbiota. *Best Pract Res Clin gastroenterol* (2013) 27:73–83. doi: 10.1016/j.bpg.2013.03.007
29. Muccioli GG, Naslain D, Backhed F, Reigstad CS, Lambert DM, Delzenne NM, et al. The endocannabinoid system links gut microbiota to adipogenesis. *Mol Syst Biol* (2010) 6:392. doi: 10.1038/msb.2010.46
30. Tian R, Wang RL, Xie H, Jin W, Yu KL. Overexpressed miRNA-155 dysregulates intestinal epithelial apical junctional complex in severe acute pancreatitis. *World J Gastroenterol WJG* (2013) 19:8282–91. doi: 10.3748/wjg.v19.i45.8282
31. Yang Y, Ma Y, Shi C, Chen H, Zhang H, Chen N, et al. Overexpression of miR-21 in patients with ulcerative colitis impairs intestinal epithelial barrier function through targeting the Rho GTPase RhoB. *Biochem Biophys Res Commun* (2013) 434:746–52. doi: 10.1016/j.bbrc.2013.03.122
32. Wang L, Zhang R, Chen J, Wu Q, Kuang Z. Baicalin Protects against TNF- α -Induced Injury by Down-Regulating miR-191a That Targets the Tight Junction Protein ZO-1 in IEC-6 Cells. *Biol Pharm Bull* (2017) 40:435–43. doi: 10.1248/bpb.b16-00789